ACS NANO

www.acsnano.org

ARTICLE

On-Surface Synthesis of a Carbon Nanoribbon Composed of 4−5−6−8-Membered Rings

Faming Kang, Luye Sun, Wenze Gao, Qiang Sun, and Wei Xu*

Cite This: *ACS Nano* 2023, 17, 8717−8722

Read Online

ACCESS | Metrics & More | Article Recommendations | Supporting Information

ABSTRACT: From the structure point of view, there are a number of ways of tiling a carbon sheet with different polygons, resulting in prospects of tailoring electronic structures of low-dimensional carbon nanomaterials. However, up to now, the experimental fabrication of such structures embedded with periodic nonhexagon carbon polygons, especially ones with more than three kinds, is still very challenging, leaving their potential properties unexplored. Here we report the bottom-up synthesis of a nanoribbon composed of 4−5−6−8-membered rings via lateral fusion of polyfluorene chains on Au(111). Scanning probe microscopy unequivocally determines both the geometric structure and the electronic properties of such a nanoribbon, revealing its semiconducting property with a bandgap of ∼1.4 eV on Au(111). We expect that this work could be helpful for designing and synthesizing complicated carbon nanoribbons.

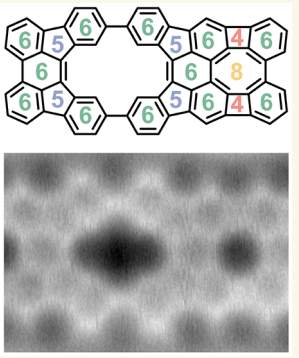

KEYWORDS: *scanning probe microscopy, on-surface synthesis, nanoribbon, nonhexagon carbon polygons, electronic structures*

Carbon affords a large number of allotropes, from zero to three dimensions, such as cyclo[*n*]carbons, fullerenes, carbyne, carbon nanotubes, graphene, graphyne, graphite, and diamond.[1] To date, various carbon allotropes have been realized and presented a variety of intriguing properties that are potentially useful in many fields.[2−6] Most remarkably, graphene[7] has attracted the most attention due to its unusual electronic[8] and magnetic properties.[9] However, its zero-bandgap property limits the potential applications in electronic and optoelectronic devices.[1] One of the efficient ways to tailor bandgap of graphene is the modification of its topology. As theoretically predicted, some graphene-derived structures, like T-graphene (4−8), pentaheptite (5−7), and phagraphene (5−6−7) with nonhexagon carbon rings exhibit metallic or gapless semimetallic behaviors.[10−16] More interestingly, special arrangement of 5−6−8-membered rings can introduce a bandgap of 0.76 eV.[17] Recently, a nonbenzenoid carbon allotrope composed of 4−6−8-membered rings has been successfully fabricated on the surface, demonstrating a metallic property.[18] Moreover, the nanoporous graphene exhibits a semiconducting characteristic.[19] Besides, laterally confining the graphene structure with certain widths[20−26] and specific edge topographies[27−29] to fabricate a series of one-dimensional graphene nanostructures, the so-called graphene nanoribbons (GNRs), has also been proved to be an efficient strategy to engineer the bandgap (as exampled in Scheme 1a). Alternatively, introducing nonhexagon carbon polygons into GNRs could provide another strategy for bandgap engineering.[30,31] Recently, GNRs embedded with such carbon polygons[18,32,33] have been successfully synthesized on surfaces (as exampled in Scheme 1b). However, up to now, among all these reported GNR nanostructures with polygons, three different polygons are incorporated in each structure at most. Therefore, it is of utmost interest to develop strategies to fabricate more complicated carbon nanoribbons with more kinds of polygons, whose potential exotic electronic and magnetic properties could be further explored.

On-surface synthesis has nowadays become a powerful strategy to fabricate precise low-dimensional carbon nanostructures. Advanced scanning probe microscopy has provided bond-resolved resolution for fine characterizations of the formed nanostructures[34] and accurate measurements of the electronic properties. Here, the precursor 2,7-diiodo-9*H*-fluorene (DIF) (as shown in Scheme 1c) was selected, in which the C−I dehalogenative coupling is expected to efficiently form one-dimensional molecular chains. Furthermore, the $-CH_2-$ groups of the fluorene could react with each other and form carbon−carbon double bond.[35] Meanwhile, the C−H sites (indicated by yellow and pink dots) undergo

Received: February 28, 2023
Accepted: April 24, 2023
Published: April 26, 2023

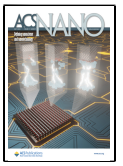

https://doi.org/10.1021/acsnano.3c01915
ACS Nano 2023, 17, 8717−8722

Scheme 1. (a, b) Structures of (a) Graphene Nanoribbon and (b) One of Its Derived Nanoribbons, Biphenylene Nanoribbon, with Nonhexagon Carbon Rings; (c) On-Surface Reactions toward the Formation of a Carbon Nanoribbon Composed of 4−5−6−8-Membered Rings

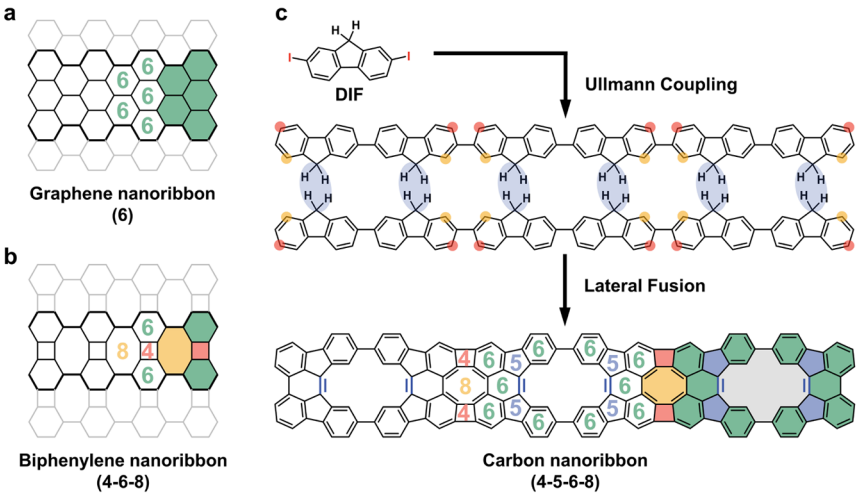

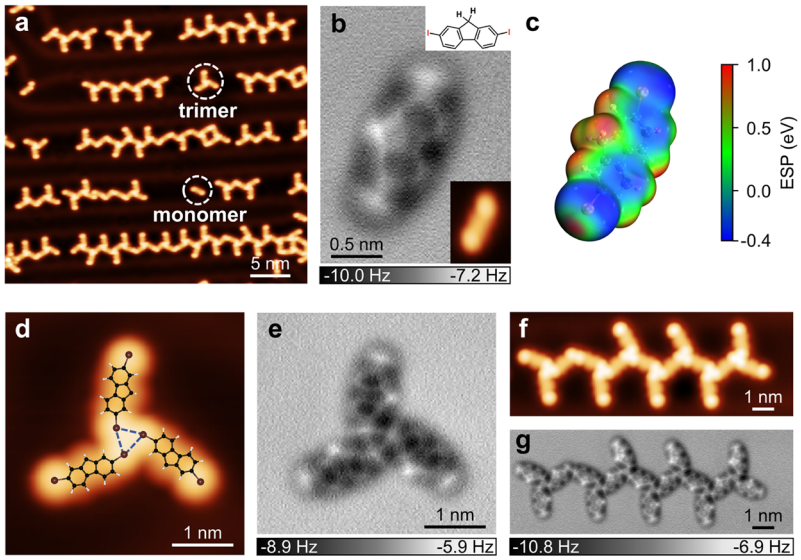

Figure 1. Self-assembly of DIF molecules on the cold Au(111) surface. (a) Large-scale STM image showing the monomer, trimer, and more complicated self-assembled structures of DIF molecules. (b) nc-AFM image of the DIF monomer with the chemical structure and an STM image as insets. (c) Calculated electrostatic potential (ESP) of a DIF molecule. The ESP is colored according to the color bar on the van der Waals surface (ρ = 0.001 a.u.) of the system. (d) STM image of the self-assembled trimer structure by halogen bonding. The relaxed model is overlaid. (e) Corresponding nc-AFM image of the DIF trimer. (f, g) STM and nc-AFM images of a self-assembled molecular chain structure based on the elementary trimer motif. All STM images were taken at V = 0.30 V, I_t = 100 pA; all nc-AFM images were recorded with a CO-functionalized tip at different tip offsets Δz (b, Δz = +50 pm; e, Δz = +10 pm; g, Δz = +30 pm) with respect to an STM set point (V = 0.30 V, I_t = 100 pA).

cyclodehydrogenation reactions, finally resulting in the formation of carbon nanoribbons specifically with four kinds of polygons, i.e., 4−5−6−8 in this case. The precise geometric structure of such a nanoribbon was unambiguously characterized by means of scanning tunneling microscopy (STM) and noncontact atomic force microscopy (nc-AFM). The electronic properties were studied by scanning tunneling spectroscopy (STS) combined with density functional theory (DFT) calculations, and this 4−5−6−8 nanoribbon shows a bandgap of about 1.4 eV on the Au(111) surface. This work may contribute a method for bandgap engineering of low-dimensional carbon nanostructures.

RESULTS AND DISCUSSION

The DIF molecules are deposited onto a cold Au(111) surface held at about 100 K. STM image (Figure 1a) exhibits the monomer, trimer, and more complicated self-assembled structures of DIF molecules. The monomer and trimer are indicated, respectively. The nc-AFM image (Figure 1b) of the monomer reveals its submolecular structure, and in particular, the $-CH_2-$ group of the fluorene appears as a bright protrusion due to its apparent height.[35−37] The calculated electrostatic potential (ESP) of a DIF molecule (Figure 1c) demonstrates both negative (blue) and positive (red) potentials at the iodine atoms due to the anisotropic

https://doi.org/10.1021/acsnano.3c01915
ACS Nano 2023, 17, 8717−8722

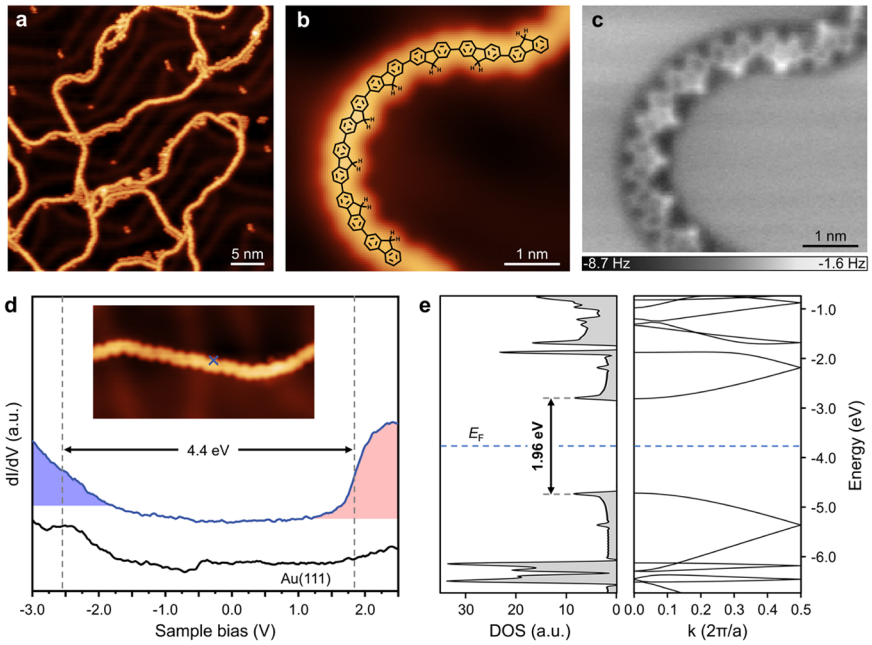

Figure 2. On-surface synthesis and characterization of the polyfluorene chain on Au(111). (a) Large-scale STM image of polyfluorene chains obtained after annealing the sample at 490 K for 30 min. (b, c) Close-up STM and nc-AFM images of a polyfluorene chain on Au(111). (d) dI/dV spectrum of the polyfluorene chain acquired at the position indicated by the blue cross (blue curve) and the reference spectrum taken on the bare Au(111) surface (black curve). The spectra are vertically shifted for clarity. (e) DFT-calculated density of states (DOS) and band structure of a freestanding polyfluorene chain. The blue dashed line indicates the Fermi level. STM images were taken at (a) V = 0.30 V, I_t = 100 pA, (b) V = −0.30 V, I_t = 100 pA, and (d) V = −0.30 V, I_t = 200 pA; the nc-AFM image in (c) was recorded with a CO-functionalized tip at tip offset Δz = 0 pm with respect to an STM set point (V = −0.30 V, I_t = 100 pA).

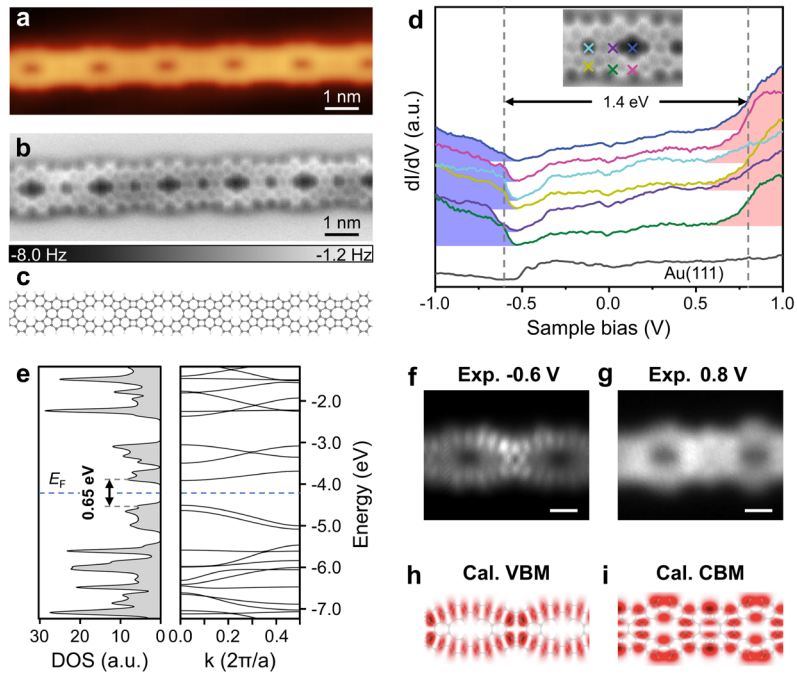

Figure 3. On-surface synthesis, characterization, and measurement of the 4−5−6−8 carbon nanoribbon on Au(111). (a, b) STM and nc-AFM images of 4−5−6−8 nanoribbon after annealing the sample at 650 K for 60 min. (c) Corresponding chemical structure of the nanoribbon. (d) dI/dV spectra of the nanoribbon acquired at different positions, indicated by the crosses with corresponding colors, and the reference spectrum taken on the bare Au(111) surface (black curve). The spectra are vertically shifted for clarity. (e) DFT-calculated DOS and band structure of the freestanding 4−5−6−8 nanoribbon. The blue dashed line indicates the Fermi level. (f, g) Constant-height dI/dV maps of the nanoribbon obtained at −0.6 and 0.8 V, respectively. Scale bars: 0.5 nm. (h, i) DFT-calculated local density of states (LDOS) maps of the valence band maximum (VBM) and the conduction band minimum (CBM) of the 4−5−6−8 nanoribbon. STM image was taken at V = −0.30 V, I_t = 100 pA; nc-AFM images (b, d) were recorded with a CO-functionalized tip at tip offset Δz = −20 pm with respect to an STM set point (V = −0.30 V, I_t = 100 pA).

https://doi.org/10.1021/acsnano.3c01915
ACS Nano 2023, 17, 8717−8722

distribution of electron density. The electrostatic interaction (halogen bonding[38−40]) between the iodine's electron-depleted cap (so-called σ-hole[41]) and encircling electron-rich belt leads to the formation of the self-assembled trimer structure as shown in the STM and nc-AFM images, respectively (Figure 1d,e). Furthermore, a more complicated self-assembled structure driven by halogen bonding, the molecular chain composed of trimer motifs, is shown in Figure 1f,g. Such chain structures prefer to grow along the herringbone reconstruction of the Au(111) substrate, as more clearly shown in the Figure S1.

Subsequent thermal annealing of the sample at 490 K for about 30 min induces dehalogenative aryl−aryl coupling reactions, resulting in the formation of one-dimensional polymers, i.e., polyfluorene chains (Figure 2a). Further close-up STM (Figure 2b) and nc-AFM (Figure 2c) images reveal the formation of individual polyfluorene chain, similar to the previously reported one,[42] whose periodicity along the chain arising from protrusions is 8.7 ± 0.2 Å (Figure S2a). The proposed model of such a polymer chain is overlaid on the STM image. As shown in the nc-AFM image (Figure 2c), the brighter contrasts at the sites of $-CH_2-$ groups in the polyfluorene chain are similar to those in the monomers, indicating that the $-CH_2-$ groups are still intact at 490 K. In addition, most $-CH_2-$ groups in Figure 2c are oriented on the same side of the polyfluorene chain, which originates from the sufficient length of such flexible polymer chains, providing the proper geometry for further lateral fusion. However, other random orientations of $-CH_2-$ groups along the polyfluorene chains are also observed (Figure S2b), like those reported in literatures.[35,42] Further, differential conductance spectroscopy (dI/dV) measurements were performed to characterize the electronic structure of the single polyfluorene chain. The dI/dV spectra shown in Figure 2d suggest a considerably large bandgap of 4.4 eV. For comparison, the DFT calculations of the band structure of free-standing polyfluorene were also performed, and the corresponding density of states (DOS) is plotted in Figure 2e, which reveals a bandgap of 1.96 eV. Notably, we did not observe other prominent peaks in the dI/dV spectrum of individual polyfluorene chain in our experimental conditions.

To induce the lateral fusion of polyfluorene chains, we further annealed the sample at 650 K for 60 min, which as expected resulted in the formation of nanoribbons as displayed in Figure 3a and the large-area STM image in Figure S3. Importantly, the nc-AFM image (Figure 3b) unambiguously resolves the fine structure of the nanoribbon, in which the 4−5−6−8-membered rings can be identified within the structure, as in the chemical model in Figure 3c and Scheme 1c. According to Scheme 1, we propose that the whole reaction pathway to the formation of 4−5−6−8 nanoribbon should start from the face-to-face dehydrogenative C−C coupling at the $-CH_2-$ sites of two polyfluorene chains, and meanwhile, cyclodehydrogenation occurs to form the corresponding 4-, 8-, and new 6-membered rings. As no −CH− groups were found in the single polyfluorene chains at 650 K, we infer that both hydrogen atoms at $-CH_2-$ sites should be removed simultaneously forming double bonds during the C−C coupling reactions (similar to ref 35). Some defects in nanoribbons are also found as reflected by STM and nc-AFM imaging (Figure S4), which are identified as unfinished cyclodehydrogenation sites (refer to the pink dots in Scheme 1c) for forming the 4-membered rings. Other side reactions, like unselective fusion reactions, are also shown in Figure S5. We note that the length of polyfluorene chains is crucial to the subsequent lateral fusion reaction. As shown in Figure S6, we also tried another precursor (2-bromo-7-iodo-9*H*-fluorene) and found that the polyfluorene chains are normally shorter than the ones formed by DIF precursor, and more importantly, no lateral fusion reaction occurred at the same experimental conditions as above. Also, no lateral fusion reaction was reported with another similar precursor (2,7-dibromo-9*H*-fluorene) in literature.[42]

The electronic structures of the 4−5−6−8 nanoribbon were explored by both scanning tunneling spectroscopy and DFT calculation. Figure 3d shows the dI/dV spectra obtained at different sites of the nanoribbon, exhibiting quite similar features in the bias voltage range from −1 to 1 V. We experimentally assign the valence band (VB) and conduction band (CB) of the nanoribbon to −0.6 and 0.8 eV, resulting in a bandgap of ∼1.4 eV. This value is again larger than the theoretical result of the free-standing ribbon with a band gap 0.65 eV (Figure 3e). Further dI/dV mapping at the corresponding bias voltages of the frontier bands (Figure 3f,g) demonstrates similar characteristics to the calculated local density of states at the band onsets (Figure 3h,i). From both dI/dV mapping and LDOS maps, we could distinguish that the local density of states shows maxima over the tetragons and octagons. We also conducted the dI/dV line scans along the lines parallel and perpendicular to the ribbon (Figure S7), and no other electronic states of interest were clearly detected.

CONCLUSIONS

We have designed a face-to-face dehydrogenative reaction of polyfluorene chains, causing their on-surface lateral fusion, and then obtained a nanoribbon containing four kinds of carbon polygons (4−5−6−8). The fine structure of the 4−5−6−8 carbon nanoribbon has been characterized by STM and nc-AFM, and the electronic property has been measured by STS, where a semiconducting bandgap of ∼1.4 eV is revealed. This work may inspire further both experimental and theoretical works toward more delicate low-dimensional carbon nanostructures with artificial bandgaps.

METHODS

All experimental measurements were carried out in a commercial (Createc) low-temperature system operated at 4.7 K with base pressure better than 1×10^{-10} mbar. Single-crystalline Au(111) surface was cleaned by several sputtering and annealing cycles. 2,7-Diiodo-9*H*-fluorene (DIF) purchased from Tansoole, Adamas, >98%, RG) and 2-bromo-7-iodo-9*H*-fluorene (purchased from Tansoole, Adamas, >98%, RG) molecules were deposited onto Au(111) surface by thermal sublimation. CO molecules for tip modification[43] were dosed onto the cold sample via a leak valve. We used a qPlus sensor[44] with a resonance frequency f_0 = 29.49 kHz, a quality factor $Q \approx$ 45,000, and a spring constant $k \approx$ 1800 N/m operated in frequency-modulation mode.[45] The bias voltage V was applied to the sample with respect to the tip. A lock-in amplifier (768 Hz, 20 mV modulation) was used to obtain dI/dV spectra and mapping. AFM images were acquired in constant-height mode at V = 0 V and an oscillation amplitude of A = 1 Å. The tip-height offsets Δz for constant-height AFM images are defined as the offset in tip−sample distance relative to the STM set point at the Au(111) surface. The positive (negative) values of Δz correspond to the tip−sample distance increased (decreased) with respect to the STM set point.

The calculations of polyfluorene chain and 4−5−6−8 nanoribbon were performed in the framework of DFT by using Vienna Ab Initio Simulation Package (VASP) code.[46,47] The projector-augmented

https://doi.org/10.1021/acsnano.3c01915
ACS Nano 2023, 17, 8717−8722

wave method was used to describe the interaction between ions and electrons,[48,49] and the Perdew–Burke–Ernzerhof generalized gradient approximation exchange–correlation functional was employed.[50] Van der Waals corrections to the PBE density functional were also included using the DFT-D3 method of Grimme.[51] The structures were relaxed until the forces were ≤0.01 eV/Å. The band structures and LDOS maps of polyfluorene chain and 4–5–6–8 nanoribbon were calculated in vacuum with the Quantum Espresso software package[52] using the PBE exchange–correlation functional.[50] The AiiDAlab web platform[53] was used to perform and manage the calculations.

The electrostatic potential calculations were carried out in the gas phase using the Gaussian 16 program package.[54] ωB97XD exchange–correlation functional[55] in conjunction with def2-TZVP basis sets[56] was used for all related calculations. The electrostatic potentials were further calculated by Multiwfn 3.8 code[57,58] combined with Visual Molecular Dynamics (VMD 1.9).[59]

ASSOCIATED CONTENT

Supporting Information

The Supporting Information is available free of charge at https://pubs.acs.org/doi/10.1021/acsnano.3c01915.

STM image of self-assembled DIF monomers; STM and nc-AFM images of polyfluorene chain; large-scale STM image of 4–5–6–8 nanoribbon; portions of different products; STM and nc-AFM images and corresponding geometric structure of the defects observed in 4–5–6–8 nanoribbons; nc-AFM images of graft areas and unselective fusion regions; STM image of polyfluorene chains synthesized by 2-bromo-7-iodo-9*H*-fluorene molecules; dI/dV line scans acquired at different points along the lines parallel and perpendicular to the 4–5–6–8 nanoribbon (PDF)

AUTHOR INFORMATION

Corresponding Author

Wei Xu – *Interdisciplinary Materials Research Center, School of Materials Science and Engineering, Tongji University, Shanghai 201804, P. R. China;* orcid.org/0000-0003-0216-794X; Email: xuwei@tongji.edu.cn

Authors

Faming Kang – *Interdisciplinary Materials Research Center, School of Materials Science and Engineering, Tongji University, Shanghai 201804, P. R. China*

Luye Sun – *Interdisciplinary Materials Research Center, School of Materials Science and Engineering, Tongji University, Shanghai 201804, P. R. China*

Wenze Gao – *Interdisciplinary Materials Research Center, School of Materials Science and Engineering, Tongji University, Shanghai 201804, P. R. China*

Qiang Sun – *Materials Genome Institute, Shanghai University, Shanghai 200444, P. R. China;* orcid.org/0000-0003-4903-4570

Complete contact information is available at: https://pubs.acs.org/10.1021/acsnano.3c01915

Notes

The authors declare no competing financial interest.

ACKNOWLEDGMENTS

The authors acknowledge the financial support from the National Natural Science Foundation of China (22125203, 21790351).

REFERENCES

(1) Georgakilas, V.; Perman, J. A.; Tucek, J.; Zboril, R. Broad family of carbon nanoallotropes: Classification, chemistry, and applications of fullerenes, carbon dots, nanotubes, graphene, nanodiamonds, and combined superstructures. *Chem. Rev.* **2015**, *115*, 4744–4822.

(2) Balandin, A. A. Thermal properties of graphene and nanostructured carbon materials. *Nat. Mater.* **2011**, *10*, 569–581.

(3) Frackowiak, E. Carbon materials for supercapacitor application. *Phys. Chem. Chem. Phys.* **2007**, *9*, 1774–1785.

(4) Chen, J.; Hamon, M. A.; Hu, H.; Chen, Y. S.; Rao, A. M.; Eklund, P. C.; Haddon, R. C. Solution properties of single-walled carbon nanotubes. *Science* **1998**, *282*, 95–98.

(5) Shvedova, A. A.; Castranova, V.; Kisin, E. R.; Schwegler-Berry, D.; Murray, A. R.; Gandelsman, V. Z.; Maynard, A.; Baron, P. Exposure to carbon nanotube material: Assessment of nanotube cytotoxicity using human keratinocyte cells. *J. Toxicol. Environ. Health A* **2003**, *66*, 1909–1926.

(6) Lin, Y.; Taylor, S.; Li, H.; Fernando, K. A. S.; Qu, L.; Wang, W.; Gu, L.; Zhou, B.; Sun, Y.-P. Advances toward bioapplications of carbon nanotubes. *J. Mater. Chem.* **2004**, *14*, 527–541.

(7) Novoselov, K. S.; Geim, A. K.; Morozov, S. V.; Jiang, D.; Zhang, Y.; Dubonos, S. V.; Grigorieva, I. V.; Firsov, A. A. Electric field effect in atomically thin carbon films. *Science* **2004**, *306*, 666–669.

(8) Castro Neto, A. H.; Guinea, F.; Peres, N. M. R.; Novoselov, K. S.; Geim, A. K. The electronic properties of graphene. *Rev. Mod. Phys.* **2009**, *81*, 109–162.

(9) Kan, E.; Li, Z.; Yang, J. Magnetism in graphene systems. *Nano* **2008**, *3*, 433–442.

(10) Crespi, V. H.; Benedict, L. X.; Cohen, M. L.; Louie, S. G. Prediction of a pure-carbon planar covalent metal. *Phys. Rev. B* **1996**, *53*, R13303–R13305.

(11) Terrones, H.; Terrones, M.; Hernandez, E.; Grobert, N.; Charlier, J. C.; Ajayan, P. M. New metallic allotropes of planar and tubular carbon. *Phys. Rev. Lett.* **2000**, *84*, 1716–1719.

(12) Liu, Y.; Wang, G.; Huang, Q.; Guo, L.; Chen, X. Structural and electronic properties of *T* graphene: A two-dimensional carbon allotrope with tetrarings. *Phys. Rev. Lett.* **2012**, *108*, 225505.

(13) Molepo, M. P.; Mapasha, R. E.; Obodo, K. O.; Chetty, N. First principles calculations of pentaheptite graphene and boronitrene derivatives. *Comput. Mater. Sci.* **2014**, *92*, 395–400.

(14) Sharma, B. R.; Manjanath, A.; Singh, A. K. Pentahexoctite: A new two-dimensional allotrope of carbon. *Sci. Rep.* **2014**, *4*, 7164.

(15) Wang, Z.; Zhou, X. F.; Zhang, X.; Zhu, Q.; Dong, H.; Zhao, M.; Oganov, A. R. Phagraphene: A low-energy graphene allotrope composed of 5–6–7 carbon rings with distorted Dirac cones. *Nano Lett.* **2015**, *15*, 6182–6186.

(16) Gu, Q.; Xing, D.; Sun, J. Superconducting single-layer T-graphene and novel synthesis routes. *Chin. Phys. Lett.* **2019**, *36*, 097401.

(17) Enyashin, A. N.; Ivanovskii, A. L. Graphene allotropes. *Phys. Status Solidi B* **2011**, *248*, 1879–1883.

(18) Fan, Q.; Yan, L.; Tripp, M. W.; Krejci, O.; Dimosthenous, S.; Kachel, S. R.; Chen, M.; Foster, A. S.; Koert, U.; Liljeroth, P.; et al. Biphenylene network: A nonbenzenoid carbon allotrope. *Science* **2021**, *372*, 852–856.

(19) Moreno, C.; Vilas-Varela, M.; Kretz, B.; Garcia-Lekue, A.; Costache, M. V.; Paradinas, M.; Panighel, M.; Ceballos, G.; Valenzuela, S. O.; Pena, D.; et al. Bottom-up synthesis of multifunctional nanoporous graphene. *Science* **2018**, *360*, 199–203.

(20) Huang, H.; Wei, D.; Sun, J.; Wong, S. L.; Feng, Y. P.; Neto, A. H.; Wee, A. T. Spatially resolved electronic structures of atomically precise armchair graphene nanoribbons. *Sci. Rep.* **2012**, *2*, 983.

(21) Ruffieux, P.; Cai, J.; Plumb, N. C.; Patthey, L.; Prezzi, D.; Ferretti, A.; Molinari, E.; Feng, X.; Muellen, K.; Pignedoli, C. A.; et al. Electronic structure of atomically precise graphene nanoribbons. *ACS Nano* **2012**, *6*, 6930–6935.

(22) Chen, Y.-C.; de Oteyza, D. G.; Pedramrazi, Z.; Chen, C.; Fischer, F. R.; Crommie, M. F. Tuning the band gap of graphene

nanoribbons synthesized from molecular precursors. *ACS Nano* **2013**, *7*, 6123−6128.
(23) Abdurakhmanova, N.; Amsharov, N.; Stepanow, S.; Jansen, M.; Kern, K.; Amsharov, K. Synthesis of wide atomically precise graphene nanoribbons from para-oligophenylene based molecular precursor. *Carbon* **2014**, *77*, 1187−1190.
(24) Basagni, A.; Sedona, F.; Pignedoli, C. A.; Cattelan, M.; Nicolas, L.; Casarin, M.; Sambi, M. Molecules-oligomers-nanowires-graphene nanoribbons: A bottom-up stepwise on-surface covalent synthesis preserving long-range order. *J. Am. Chem. Soc.* **2015**, *137*, 1802−1808.
(25) Zhang, H.; Lin, H.; Sun, K.; Chen, L.; Zagranyarski, Y.; Aghdassi, N.; Duhm, S.; Li, Q.; Zhong, D.; Li, Y.; et al. On-surface synthesis of rylene-type graphene nanoribbons. *J. Am. Chem. Soc.* **2015**, *137*, 4022−4025.
(26) Talirz, L.; Sode, H.; Dumslaff, T.; Wang, S.; Sanchez-Valencia, J. R.; Liu, J.; Shinde, P.; Pignedoli, C. A.; Liang, L.; Meunier, V.; et al. On-surface synthesis and characterization of 9-atom wide armchair graphene nanoribbons. *ACS Nano* **2017**, *11*, 1380−1388.
(27) Cai, J.; Ruffieux, P.; Jaafar, R.; Bieri, M.; Braun, T.; Blankenburg, S.; Muoth, M.; Seitsonen, A. P.; Saleh, M.; Feng, X.; et al. Atomically precise bottom-up fabrication of graphene nanoribbons. *Nature* **2010**, *466*, 470−473.
(28) Ruffieux, P.; Wang, S.; Yang, B.; Sanchez-Sanchez, C.; Liu, J.; Dienel, T.; Talirz, L.; Shinde, P.; Pignedoli, C. A.; Passerone, D.; et al. On-surface synthesis of graphene nanoribbons with zigzag edge topology. *Nature* **2016**, *531*, 489−492.
(29) de Oteyza, D. G.; Garcia-Lekue, A.; Vilas-Varela, M.; Merino-Diez, N.; Carbonell-Sanroma, E.; Corso, M.; Vasseur, G.; Rogero, C.; Guitian, E.; Pascual, J. I.; et al. Substrate-independent growth of atomically precise chiral graphene nanoribbons. *ACS Nano* **2016**, *10*, 9000−9008.
(30) Liu, M.; Liu, M.; She, L.; Zha, Z.; Pan, J.; Li, S.; Li, T.; He, Y.; Cai, Z.; Wang, J.; et al. Graphene-like nanoribbons periodically embedded with four- and eight-membered rings. *Nat. Commun.* **2017**, *8*, 14924.
(31) Li, D. Y.; Qiu, X.; Li, S. W.; Ren, Y. T.; Zhu, Y. C.; Shu, C. H.; Hou, X. Y.; Liu, M.; Shi, X. Q.; Qiu, X.; et al. Ladder phenylenes synthesized on Au(111) surface via selective [2 + 2] cycloaddition. *J. Am. Chem. Soc.* **2021**, *143*, 12955−12960.
(32) Fan, Q.; Martin-Jimenez, D.; Ebeling, D.; Krug, C. K.; Brechmann, L.; Kohlmeyer, C.; Hilt, G.; Hieringer, W.; Schirmeisen, A.; Gottfried, J. M. Nanoribbons with nonalternant topology from fusion of polyazulene: Carbon allotropes beyond graphene. *J. Am. Chem. Soc.* **2019**, *141*, 17713−17720.
(33) Sun, Q.; Hou, I. C.; Eimre, K.; Pignedoli, C. A.; Ruffieux, P.; Narita, A.; Fasel, R. On-surface synthesis of polyazulene with 2,6-connectivity. *Chem. Commun.* **2019**, *55*, 13466−13469.
(34) Gross, L.; Mohn, F.; Moll, N.; Liljeroth, P.; Meyer, G. The chemical structure of a molecule resolved by atomic force microscopy. *Science* **2009**, *325*, 1110−1114.
(35) Di Giovannantonio, M.; Eimre, K.; Yakutovich, A. V.; Chen, Q.; Mishra, S.; Urgel, J. I.; Pignedoli, C. A.; Ruffieux, P.; Mullen, K.; Narita, A.; et al. On-surface synthesis of antiaromatic and open-shell indeno[2,1-*b*]fluorene polymers and their lateral fusion into porous ribbons. *J. Am. Chem. Soc.* **2019**, *141*, 12346−12354.
(36) Mallada, B.; de la Torre, B.; Mendieta-Moreno, J. I.; Nachtigallova, D.; Matej, A.; Matousek, M.; Mutombo, P.; Brabec, J.; Veis, L.; Cadart, T.; et al. On-surface strain-driven synthesis of nonalternant non-benzenoid aromatic compounds containing four- to eight-membered rings. *J. Am. Chem. Soc.* **2021**, *143*, 14694−14702.
(37) Zhao, Y.; Jiang, K.; Li, C.; Liu, Y.; Zhu, G.; Pizzochero, M.; Kaxiras, E.; Guan, D.; Li, Y.; Zheng, H.; et al. Quantum nanomagnets in on-surface metal-free porphyrin chains. *Nat. Chem.* **2023**, *15*, 53.
(38) Han, Z.; Czap, G.; Chiang, C.-L.; Xu, C.; Wagner, P. J.; Wei, X.; Zhang, Y.; Wu, R.; Ho, W. Imaging the halogen bond in self-assembled halogenbenzenes on silver. *Science* **2017**, *358*, 206−210.
(39) Li, S.; Duan, S.; Zha, Z.; Pan, J.; Sun, L.; Liu, M.; Deng, K.; Xu, X.; Qiu, X. Structural phase transitions of molecular self-assembly driven by nonbonded metal adatoms. *ACS Nano* **2020**, *14*, 6331−6338.
(40) Tschakert, J.; Zhong, Q.; Martin-Jimenez, D.; Carracedo-Cosme, J.; Romero-Muniz, C.; Henkel, P.; Schloder, T.; Ahles, S.; Mollenhauer, D.; Wegner, H. A.; et al. Surface-controlled reversal of the selectivity of halogen bonds. *Nat. Commun.* **2020**, *11*, 5630.
(41) Clark, T.; Hennemann, M.; Murray, J. S.; Politzer, P. Halogen bonding: the σ-hole. *J. Mol. Model.* **2007**, *13*, 291−296.
(42) Xiong, W.; Lu, J.; Geng, J.; Ruan, Z.; Zhang, H.; Zhang, Y.; Niu, G.; Fu, B.; Zhang, Y.; Sun, S.; et al. Atomic-scale construction and characterization of quantum dots array and poly-fluorene chains via 2,7-dibromofluorene on Au(111). *Appl. Surf. Sci.* **2023**, *609*, 155315.
(43) Gross, L.; Mohn, F.; Moll, N.; Liljeroth, P.; Meyer, G. The chemical structure of a molecule resolved by atomic force microscopy. *Science* **2009**, *325*, 1110−1114.
(44) Giessibl, F. J. High-speed force sensor for force microscopy and profilometry utilizing a quartz tuning fork. *Appl. Phys. Lett.* **1998**, *73*, 3956−3958.
(45) Albrecht, T. R.; Grütter, P.; Horne, D.; Rugar, D. Frequency modulation detection using high-Q cantilevers for enhanced force microscope sensitivity. *J. Appl. Phys.* **1991**, *69*, 668−673.
(46) Kresse, G.; Hafner, J. Ab initio molecular dynamics for open-shell transition metals. *Phys. Rev. B: Condens. Matter Mater. Phys.* **1993**, *48*, 13115−13118.
(47) Kresse, G.; Furthmüller, J. Efficient iterative schemes for ab initio total-energy calculations using a plane-wave basis set. *Phys. Rev. B: Condens. Matter Mater. Phys.* **1996**, *54*, 11169−11186.
(48) Blöchl, P. E. Projector augmented-wave method. *Phys. Rev. B: Condens. Matter Mater. Phys.* **1994**, *50*, 17953−17979.
(49) Kresse, G.; Joubert, D. From ultrasoft pseudopotentials to the projector augmented-wave method. *Phys. Rev. B: Condens. Matter Mater. Phys.* **1999**, *59*, 1758−1775.
(50) Perdew, J. P.; Burke, K.; Ernzerhof, M. Generalized gradient approximation made simple. *Phys. Rev. Lett.* **1996**, *77*, 3865−3868.
(51) Grimme, S.; Antony, J.; Ehrlich, S.; Krieg, H. A consistent and accurate ab initio parametrization of density functional dispersion correction (DFT-D) for the 94 elements H-Pu. *J. Chem. Phys.* **2010**, *132*, 154104.
(52) Giannozzi, P.; Baroni, S.; Bonini, N.; Calandra, M.; Car, R.; Cavazzoni, C.; Ceresoli, D.; Chiarotti, G. L.; Cococcioni, M.; Dabo, I.; et al. QUANTUM ESPRESSO: A modular and open-source software project for quantum simulations of materials. *J. Phys.: Condens. Matter* **2009**, *21*, 395502.
(53) Yakutovich, A. V.; Eimre, K.; Schütt, O.; Talirz, L.; Adorf, C. S.; Andersen, C. W.; Ditler, E.; Du, D.; Passerone, D.; Smit, B.; et al. AiiDAlab - an ecosystem for developing, executing, and sharing scientific workflows. *Comput. Mater. Sci.* **2021**, *188*, 110165.
(54) Frisch, M. J.; Trucks, G. W.; Schlegel, H. B.; Scuseria, G. E.; Robb, M. A.; Cheeseman, J. R.; Scalmani, G.; Barone, V.; Petersson, G. A.; Nakatsuji, H.; et al. *Gaussian 16*, rev. C.01; Gaussian, Inc.: Wallingford, CT, 2016.
(55) Chai, J. D.; Head-Gordon, M. Long-range corrected hybrid density functionals with damped atom-atom dispersion corrections. *Phys. Chem. Chem. Phys.* **2008**, *10*, 6615−6620.
(56) Weigend, F.; Ahlrichs, R. Balanced basis sets of split valence, triple zeta valence and quadruple zeta valence quality for H to Rn: design and assessment of accuracy. *Phys. Chem. Chem. Phys.* **2005**, *7*, 3297−3305.
(57) Lu, T.; Chen, F. Multiwfn: a multifunctional wavefunction analyzer. *J. Comput. Chem.* **2012**, *33*, 580−592.
(58) Zhang, J.; Lu, T. Efficient evaluation of electrostatic potential with computerized optimized code. *Phys. Chem. Chem. Phys.* **2021**, *23*, 20323−20328.
(59) Humphrey, W.; Dalke, A.; Schulten, K. VMD: visual molecular dynamics. *J. Mol. Graphics* **1996**, *14*, 33−38.

https://doi.org/10.1021/acsnano.3c01915
ACS Nano 2023, 17, 8717−8722